

Fast Cross-Correlation for TDoA Estimation on Small Aperture Microphone Arrays

François Grondin, Marc-Antoine Maheux, Jean-Samuel Lauzon, Jonathan Vincent, François Michaud

Abstract—This paper introduces the Fast Cross-Correlation (FCC) method for Time Difference of Arrival (TDoA) Estimation for pairs of microphones on a small aperture microphone array. FCC relies on low-rank decomposition and exploits symmetry in even and odd bases to speed up computation while preserving TDoA accuracy. FCC reduces the number of flops by a factor of 4.5 and the execution speed by factors of 8.2, 2.6 and 2.7 on a Raspberry Pi Zero, a Raspberry Pi 4 and a Nvidia Jetson TX2 devices, respectively, compared to the state-of-the-art Generalized Cross-Correlation (GCC) method that relies on the Fast Fourier Transform (FFT). This improvement can provide portable microphone arrays with extended battery life and allow real-time processing on low-cost hardware.

Index Terms—Time Difference of Arrival, Fast Cross-Correlation, Generalized Cross-Correlation, Microphone Array, Sound Source Localization

I. INTRODUCTION

MANY smart devices (e.g., smart speakers, tablets, cell phones) are now equipped with multiple microphones to perform sound source localization and speech enhancement [1], [2]. Using multiple microphones come particularly handy to cope with performance drop for distant speech recognition tasks [3]. While many devices still perform sound recognition tasks on the cloud, there is a growing need for local processing on the device, to reduce bandwidth usage, minimize latency and protect privacy. This requires to revisit some algorithms to reduce the computational load and extend battery life for portable devices.

Sound source localization (SSL) consists in estimating the direction of arrival (DoA) of sound using multiple microphones positioned in a specific geometrical configuration [4], [5]. DoA information is useful for audio scene analysis [6], [7] and can be used with beamforming methods [8], [9], [10], [11] to enhance the target source and reduce interference. DoA can also solve the permutation ambiguity in speech separation tasks [12] with multiple microphones, in deep clustering for instance [13], [14], [15] or time-frequency masking [16], [17], [18]. SSL can also serve numerous applications in robotics [19], ranging from acoustic synchronous localization and mapping (SLAM) [20], rescue missions [21], [22], drones tracking [23], [24], [25] and assisting humans with hearing impairments [26]. Some frameworks have been proposed over the years to perform online SSL on robots [27], [28].

F. Grondin, M.-A. Maheux, J.-S. Lauzon, J. Vincent and F. Michaud are with the Department of Electrical Engineering and Computer Engineering, Université de Sherbrooke (Québec, Canada) e-mail: {francois.grondin2, marc-antoine.maheux, jean-samuel.lauzon, jonathan.vincent2, francois.michaud}@usherbrooke.ca.

There are three main categories of SSL methods: 1) beamforming, 2) subspace decomposition, and 3) machine learning approaches. SSL with beamforming consists in pointing a beam at potential DoAs around the microphone array to find the direction that captures the most power. This is usually achieved using a Steered-Response Power Phase Transform beamformer, referred to SRP-PHAT [29], [30]. It is common to compute SRP-PHAT using the Generalized Cross-Correlation with Phase Transform (GCC-PHAT) applied to each pair of microphones [31], [32], [33], [34]. However, scanning every possible DoA to find the most likely candidate involve numerous lookups, especially when performing 3-D localization. To cope with this challenge, a two-level resolution scanning grid can be used [35]. The SMP-PHAT method exploits the symmetry of the microphone array to reduce the number of computations [36]. It is also possible to use the SVD-PHAT method, which relies on Singular Value Decomposition of the SRP-PHAT projection matrix [37], [38]. Once the principal components are estimated, a k-d tree is used to speed up the search for the most likely DoA of sound. SVD-PHAT however requires to compute offline a decomposition for each specific microphone geometry, which can be computationally expensive for arrays with numerous microphones, or if the shape changes dynamically over time.

Subspace decomposition methods include Multiple Signal Classification (MUSIC) [39] and Estimation of Signal Parameters via Rotational Invariant Techniques (ESPRIT) [40]. While MUSIC was initially used for narrowband signals, it was adapted to broadband signals like speech, and can be defined as Standard Eigenvalue Decomposition MUSIC (SEVD-MUSIC) [41], [42]. SEVD-MUSIC assumes the speech signal is more powerful than noise at each frequency bin, which is usually not the case. Nakamura et al. introduced the MUSIC based on Generalized Eigenvalue Decomposition (GEVD-MUSIC) method to overcome this limitation [43], [44], [45]. While this method handles cases where noise is more powerful than speech, it also introduces some localization errors because the generated noise subspace is made of correlated bases. To deal with this issue, Generalized Singular Value Decomposition (GSVD-MUSIC) enforces orthogonality between the noise subspace bases and thus improves the DoA estimation accuracy [46]. All MUSIC-based methods rely on online eigenvalue or singular value decompositions that are computationally expensive, and make on-board real-time processing challenging.

Machine learning approaches usually involve training a deep neural network with a specific array geometry and predict a class amongst all classes that stand for all potential DoAs.

Chakrabarty and Habets [47], [48] demonstrate that a convolutional neural network (CNN) could be trained on white noise signals to estimate the DoA for a Uniform Linear Array (ULA). Other approaches also demonstrate the robustness of CNNs and fully connecter networks in low signal-to-noise ratio (SNR) scenarios [49], [50], [51], [52]. Çakir et al. [53] showed that convolutive and recursive neural networks (CRNNs) could be used for sound event detection, followed by Adavanne et al. [54], [55] who demonstrated CRNNs could estimate the DoAs for a specific class of sound. It is also possible to estimate the TDoAs for each pair of microphones for a specific class of sound using CRNNs [56]. While most deep-learning-based approaches outperform traditional signal processing methods in terms of accuracy, they involve a significant amount of computations due to the numerous parameters in their layers, which makes them less suitable for real-time applications on low-cost embedded hardware.

This paper presents a novel method to estimate the time difference of arrival (TDoA), called Fast Cross-Correlation (FCC), specifically adapted to microphone arrays with small aperture (a few centimeters) with limited available computing capacity. As sound source localization is often performed locally on low-cost hardware, this method offers an interesting alternative to the existing generalized cross-correlation (GCC) approach as it reduces considerably the amount of computations. FCC is inspired by the former SVD-PHAT method [37], yet it involves additional improvements due to the symmetry made possible by considering each pair of microphones individually. The two main contributions of this paper are: 1) it describes the FCC method and demonstrates it reduces the theoretical amount of flops compared to the GCC approach; 2) it explains FCC implementation in the C language and demonstrates its superior performance in term of execution time on a Raspberry Pi Zero [57], a Raspberry Pi 4 [58] and a Nvidia Jetson TX2 [59] devices, compared to GCC computed using the state-of-the-art optimized Fast Fourier Transform (FFT) library FFTW [60].

II. TIME DIFFERENCE OF ARRIVAL

The Time Difference of Arrival (TDoA) of sound corresponds to the time delay due to the propagation of sound in air between two microphones. This delay is typically expressed in seconds, but it is often convenient to measure it in samples when dealing with discrete-time signals. For a given direction of arrival (DoA) of sounds denoted by the angle $\theta \in [0, \pi]$ in radians, the TDoA (in samples) corresponds to:

$$\tau = f_S \left(\frac{d}{c} \right) \cos \theta, \quad (1)$$

where $c \in \mathbb{R}^+$ stands for the speed of sound (in m/sec), $d \in \mathbb{R}^+$ for the distance between both microphones (in m), $f_S \in \mathbb{N}$ for the sample rate (in samples/sec) and $\tau \in [-\tau_{max}, +\tau_{max}]$ for the TDoA, where $\tau_{max} = df_S/c$. TDoA estimation can be achieved by computing the correlation between both microphone signals to find the suitable phase shift that aligns both signals.

Figure 1 shows the overall processing pipeline to estimate the TDoA from the signals of two microphones. We define

$x_1[n] \in \mathbb{R}$ and $x_2[n] \in \mathbb{R}$ as the signals in the time-domain for two microphones (denoted here as 1 and 2), where $n \in \mathbb{N}$ stands for the sample index. A Short-Time Fourier Transform (STFT) with a frame size of $N \in \{2, 4, 8, 16, \dots\}$ samples (power of 2 for radix-2 FFT) is performed on each signal. Typically this STFT uses a Hann window and an overlap of 50% between frames. This generates the frames $X_1(t, f) \in \mathbb{C}$ and $X_2(t, f) \in \mathbb{C}$, where $t \in \{1, 2, \dots, T\}$ stands for the time index, $T \in \mathbb{N}$ for the number of frames, and $f \in \{0, 1, \dots, N/2\}$ for the frequency bin index (for real input signals, the spectrum is symmetric after bin $N/2$, and thus the bins between indices $N/2+1$ and N can be ignored). The cross-spectrum $R(t, f) \in \mathbb{C}$ between microphones 1 and 2 can be estimated recursively over time, using a smoothing factor defined by the parameter $\alpha \in [0, 1]$:

$$R(t, f) = (1 - \alpha)R(t - 1, f) + \alpha X_1(t, f)X_2(t, f)^*, \quad (2)$$

where $\{\dots\}^*$ stands the complex conjugate.

The phase transform is then applied to normalize the cross-spectrum:

$$\hat{R}(t, f) = \frac{R(t, f)}{|R(t, f)|}, \quad (3)$$

where the division by the absolute value $|\dots|$ performs the phase transform.

From now on we can omit the index t for clarity (so $\hat{R}(t, f)$ becomes $\hat{R}(f)$), without loss of generality. The expression $y(\tau)$ stands for the cross-correlation (computed on $\hat{R}(f)$, either with GCC or FCC) between the signals for each candidate delay $\tau \in \{\tau_1, \tau_2, \dots, \tau_I\}$, where I stands for the number of candidates. The goal is to find the delay that maximizes the correlation $y(\tau)$ between both signals:

$$\tau^* = \arg \max_{\tau} \{y(\tau)\}. \quad (4)$$

Once the most likely TDoA (denoted as τ^*) is found, a polynomial interpolation is applied to improve accuracy. There exist numerous interpolation methods, but here we limit ourselves to quadratic interpolation, as it requires little computation and a closed-form solution exists [61]. A more accurate TDoA $\hat{\tau}$ can therefore be obtained by using the target TDoA τ^* and its neighbours ($\tau^* - \Delta\tau$ and $\tau^* + \Delta\tau$):

$$\hat{\tau} = \tau^* + \frac{\Delta\tau}{2} \left(\frac{y(\tau^* - \Delta\tau) - y(\tau^* + \Delta\tau)}{y(\tau^* - \Delta\tau) - 2y(\tau^*) + y(\tau^* + \Delta\tau)} \right), \quad (5)$$

where $\Delta\tau$ is the interval between two consecutive delays.

III. GENERALIZED CROSS-CORRELATION

The Generalized Cross-Correlation is widely used for TDoA estimation and is appealing as it relies on the well-known Fast Fourier Transform (FFT) algorithm. The cross-correlation is computed as follows:

$$y(\tau) = 2\Re \left\{ \sum_{f=0}^{N/2} \hat{R}(f) \exp(j2\pi f\tau/N) \right\}, \quad (6)$$

where $\Re\{\dots\}$ captures the real part.

A real-valued Inverse Fast Fourier Transform (IFFT) can be used to compute efficiently the expression in (6). However,

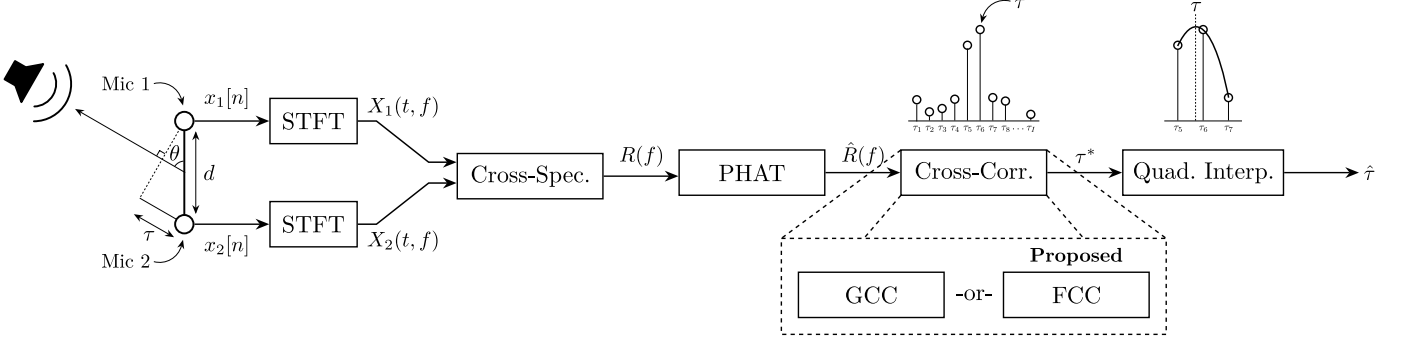


Fig. 1. TDoA estimation, using either the traditional method (GCC) or the proposed approach (FCC).

according to the Discrete Fourier Transform (DFT) definition, it assumes that τ is an integer, which reduces considerably the number of TDoA candidates, especially when the distance d between both microphones is small (and so is τ_{max} , as shown in (1)). This also becomes an issue for quadratic interpolation, as there is only one discrete delay value that samples the main lobe. The solution to this limitation consists in performing an IFFT twice the size of the input frame. This is achieved by padding the frame with zeros to double the number of frequency bins ($r = 2$) prior to computing the IFFT. This results in time-domain interpolation, with a resolution of 0.5 sample (or more generally, $1/r$ sample). Figure 2 illustrates how this operation allows sampling the main lobe properly for accurate estimation of the TDoA with quadratic interpolation. This interpolation also implies there are $I = 4\lceil\tau_{max}\rceil + 1$ delay candidates, where $\lceil \dots \rceil$ stands for the ceiling operator. For example, to accommodate for distance up to $d = 0.15$ m between microphones for a sample rate of $f_S = 16000$ samples/sec and speed of sound $c = 343.0$ m/sec, $\tau_{max} = 8$ and this results in $I = 33$ candidates.

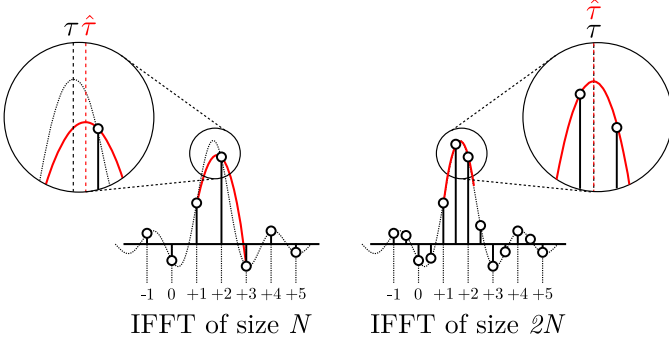


Fig. 2. Quadratic interpolation without (size of N) and with (size of $2N$) interpolation.

Performing time-domain interpolation can however become an issue for real-time systems as the computational load increases when the IFFT size gets larger. Although the exact number of flops depends on the specific FFT algorithm implementation, it is in the order of $5N/r \log_2(rN)$ for radix-2 implementation with real numbers and rN samples [60]. For example, with a frame size of $N = 512$ and a factor of $r = 2$, GCC requires approximately 25600 flops. While the FFT provides efficient computation for GCC, there is still

room for improvement, as will be demonstrated with the Fast Cross-Correlation approach.

IV. FAST CROSS-CORRELATION

Figure 3 shows the pipeline of the proposed FCC approach. Equation 6 is formulated in vector form in this section to ease the description of FCC. All the cross-spectrum coefficients with phase transform can be stacked for all frequency bins ($f \in \{0, 1, \dots, N/2\}$) in a single vector called $\mathbf{x} \in \mathbb{C}^{N/2+1}$:

$$\mathbf{x} = \begin{bmatrix} \hat{R}(0) \\ \hat{R}(1) \\ \vdots \\ \hat{R}(N/2) \end{bmatrix}. \quad (7)$$

Similarly, all the beamformer coefficients $w(\tau, f) = \exp(j2\pi f\tau/N)$ are concatenated in a vector $\mathbf{w}(\tau) \in \mathbb{C}^{N/2+1}$:

$$\mathbf{w}(\tau) = [w(\tau, 0) \ w(\tau, 1) \ \dots \ w(\tau, N/2)]. \quad (8)$$

The vectors can be combined in a matrix $\mathbf{W} \in \mathbb{C}^{I \times N/2+1}$ as follows:

$$\mathbf{W} = \begin{bmatrix} \mathbf{w}(\tau_1) \\ \mathbf{w}(\tau_2) \\ \vdots \\ \mathbf{w}(\tau_I) \end{bmatrix}. \quad (9)$$

The expression initially introduced in (6) can therefore be represented in matrix form:

$$\mathbf{y} = 2\Re\{\mathbf{W}\mathbf{x}\}, \quad (10)$$

where the vector $\mathbf{y} \in \mathbb{C}^I$ corresponds to the cross-correlation $y(\tau)$ for each delay $\tau \in \{\tau_1, \tau_2, \dots, \tau_I\}$ (where the number of candidates corresponds to the same value obtained with GCC, that is $I = 4\lceil\tau_{max}\rceil + 1$):

$$\mathbf{y} = \begin{bmatrix} y(\tau_1) \\ y(\tau_2) \\ \vdots \\ y(\tau_I) \end{bmatrix}. \quad (11)$$

The expression in (10) involves $I(N/2+1)$ complex multiplications, and $IN/2$ complex additions. Each complex multiplication involves 4 real multiplications, and 2 real additions, while each complex addition requires 2 real additions. This

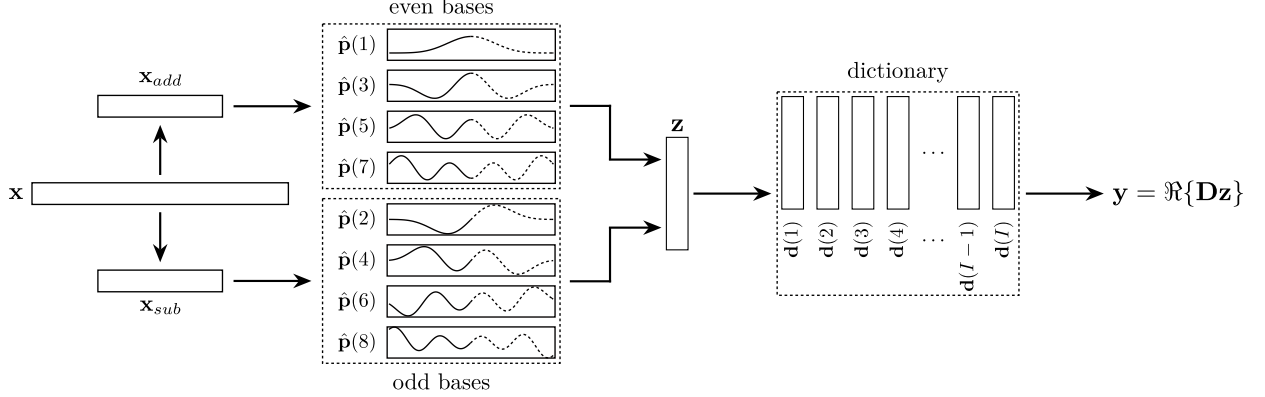


Fig. 3. Overview of the FCC-PHAT approach. The input vector is first divided in two smaller vectors, \mathbf{x}_{add} and \mathbf{x}_{sub} , which are used to perform the dot product with the even and odd bases from the matrix \mathbf{P} . The result is a dense vector, denoted as \mathbf{z} , which is projected on each element of the dictionary \mathbf{D} to generate the cross-correlation vector \mathbf{y} .

sums up to $I(4N + 6)$ flops, which can be prohibitive for real-time applications when the number of candidates I gets large. With $\tau_{max} = 8$ and frame size of $N = 512$ samples, the direct computation of (10) involves 67782 flops. This is more flops than with GCC, which suggests further optimization is required.

As explored previously in [37], the matrix \mathbf{W} is usually low-rank, especially when the distance d between the microphones is small, i.e., in the order of a few centimeters. This matrix can be factored using singular value decomposition (SVD), which leads to the following equation:

$$\mathbf{W} = \mathbf{U}\mathbf{S}\mathbf{V}^H \quad (12)$$

where $\mathbf{U} \in \mathbb{C}^{I \times I}$, $\mathbf{S} \in \mathbb{R}^{I \times N/2+1}$, $\mathbf{V} \in \mathbb{C}^{N/2+1 \times N/2+1}$ and $\{\dots\}^H$ stands for the Hermitian transpose operator.

As shown in [37], the matrices can be cropped by keeping only the K most significant singular values. This leads to matrices $\hat{\mathbf{U}} \in \mathbb{C}^{I \times K}$, $\hat{\mathbf{S}} \in \mathbb{R}^{K \times K}$ and $\hat{\mathbf{V}} \in \mathbb{C}^{N/2+1 \times K}$, such that $\mathbf{W} \approx \hat{\mathbf{U}}\hat{\mathbf{S}}\hat{\mathbf{V}}^H$. The parameter K is chosen to ensure accurate reconstruction of \mathbf{W} , to be set experimentally. For now, we assume K is known and the projection matrix $\mathbf{P} \in \mathbb{C}^{K \times N/2+1}$ is defined as:

$$\mathbf{P} = \hat{\mathbf{S}}\hat{\mathbf{V}}^H, \quad (13)$$

and the dictionary as:

$$\mathbf{D} = \hat{\mathbf{U}}. \quad (14)$$

The dictionary can be seen as a concatenation of rows $\mathbf{d}(i) \in \mathbb{C}^{1 \times K}$ for each TDoA candidate τ_i . The cross-correlation can thus be estimated as follows:

$$\mathbf{y} = 2\Re\{\mathbf{D}\mathbf{z}\}, \quad (15)$$

where $\mathbf{z} = \mathbf{Px}$. At this point, computing \mathbf{z} involves $K(N/2 + 1)$ complex multiplications, and $KN/2$ complex additions, for a total of $K(4N + 6)$ flops. The computation of $2\Re\{\mathbf{D}\mathbf{z}\}$ then involves $2IK$ real multiplications, and $I(2K - 1)$ real additions, for a total of $4KI - I$ flops. This sums up to $K(4N + 6) + I(4K - 1)$ flops, which leads approximately to a computational load reduction by a factor of N/K compared to the former expression in (10) when $I \ll N$. With the previous example ($\tau_{max} = 8$ so $I = 33$, and $N = 512$), and by

choosing $K = 8$, the number of flops goes down to 17455 (compared to 67782).

While this reduction definitely helps (and now involves around 32% less flops than GCC), it still remains expensive and similar to GCC. It is possible to reduce it further by exploiting some properties that emerged from the bases generated by low-rank reduction. To describe this, the projection matrix \mathbf{P} is expressed as K concatenated vectors:

$$\mathbf{P} = \begin{bmatrix} \mathbf{p}(1) \\ \mathbf{p}(2) \\ \vdots \\ \mathbf{p}(K) \end{bmatrix}, \quad (16)$$

where:

$$\mathbf{p}(k) = [p(k, 0) \ p(k, 1) \ \dots \ p(k, N/2)]. \quad (17)$$

We observe that all the bases are either even and real, or odd and purely imaginary with respect to the frequency bins, such that:

$$p(k, f) = \begin{cases} +p(k, N/2 - f) & k = \{1, 3, 5, \dots\} \\ -p(k, N/2 - f) & k = \{2, 4, 6, \dots\} \end{cases}, \quad (18)$$

where $p(k, f) \in \mathbb{R}$ when $k \in \{1, 3, 5, \dots\}$, and $p(k, f) \in j\mathbb{R}$ when $k \in \{2, 4, 6, \dots\}$. Figure 4 presents an example of this property when $\tau_{max} = 8$ and $N = 512$.

Because the bases $\mathbf{p}(k) \in \mathbb{C}^{N/2+1}$ are even or odd, the second half is redundant and the vectors can be cropped to smaller bases $\hat{\mathbf{p}}(k) \in \mathbb{C}^{N/4+1}$:

$$\hat{\mathbf{p}}(k) = [p(k, 0) \ p(k, 1) \ \dots \ p(k, N/4)]. \quad (19)$$

To compute \mathbf{z} , the initial frame $\mathbf{x} \in \mathbb{C}^{N/2+1}$ can be reorganized as the sum (\mathbf{x}_{add}) and difference (\mathbf{x}_{sub}) of the cross-spectrum coefficients (\mathbf{x}):

$$\mathbf{x}_{add} = \begin{bmatrix} \hat{R}(0) + \hat{R}(N/2) \\ \hat{R}(1) + \hat{R}(N/2 - 1) \\ \vdots \\ \hat{R}(N/4 - 1) + \hat{R}(N/4 + 1) \\ \hat{R}(N/4) \end{bmatrix}, \quad (20)$$

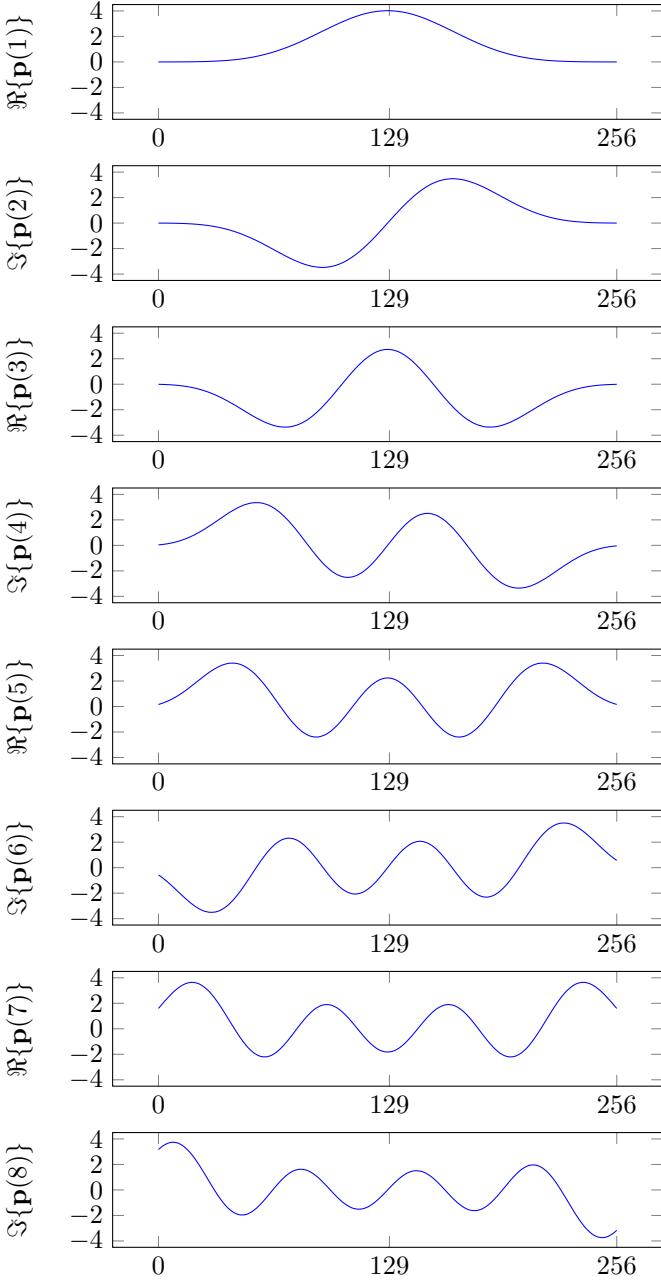


Fig. 4. Bases $\mathbf{p}(k)$ for $k \in \{1, 2, \dots, 8\}$ with $\tau_{max} = 8$ and $N = 512$, where the bases with $k \in \{1, 3, \dots, 7\}$ are even and real, and the ones with $k \in \{2, 4, \dots, 8\}$ are odd and purely imaginary. Here $\Re\{\dots\}$ and $\Im\{\dots\}$ extracts the real and imaginary part, respectively.

$$\mathbf{x}_{sub} = \begin{bmatrix} \hat{R}(0) - \hat{R}(N/2) \\ \hat{R}(1) - \hat{R}(N/2 - 1) \\ \vdots \\ \hat{R}(N/4 - 1) - \hat{R}(N/4 + 1) \\ \hat{R}(N/4) \end{bmatrix}. \quad (21)$$

Note that because the number of elements is odd ($N/2 + 1$), the element in the middle (at $N/4 + 1$) stands alone. Also, computing \mathbf{x}_{add} and \mathbf{x}_{sub} only needs to be performed once for a given \mathbf{x} , and can be stored in cache memory and reused multiple times. This new formulation then implies that \mathbf{z} can

be computed as follows:

$$\mathbf{z} = \begin{bmatrix} \hat{\mathbf{p}}(1) \\ \hat{\mathbf{p}}(2) \\ \hat{\mathbf{p}}(3) \\ \hat{\mathbf{p}}(4) \\ \vdots \end{bmatrix} \begin{bmatrix} \mathbf{x}_{add} & \mathbf{x}_{sub} & \mathbf{x}_{add} & \mathbf{x}_{sub} & \dots \end{bmatrix}. \quad (22)$$

The bases now hold $N/4 + 1$ elements (instead of $N/2 + 1$) and all the elements of $\hat{\mathbf{p}}(k)$ are purely real or imaginary numbers. Computing (22) involves $K(N/2 + 2)$ real multiplications and $KN/2$ real additions, for a total of $K(N + 2)$ flops. Computing the vectors $\mathbf{x}_{add}(t)$ and $\mathbf{x}_{sub}(t)$ also adds N flops, which leads to a total of $K(N + 2) + N$ flops. Performing the operation \mathbf{Dz} then adds $I(4K - 1)$ flops, as mentioned earlier. This leads to $K(N + 2) + N + I(4K - 1)$ flops in total. With the previous example ($\tau_{max} = 8$ so $I = 33$, and $N = 512$), the number of flops drops to 5647, which now represents a significant gain by a factor of 4.5 compared to GCC (25600 flops).

Table I summarizes the number of flops for each method. It is interesting to note that while GCC has a complexity of $\mathcal{O}(N \log N)$, FCC exhibits a linear behaviour $\mathcal{O}(N)$. The next section examines how this gain in performance influences TDoA accuracy and the number of computations.

TABLE I
COMPUTATIONAL LOAD FOR EACH METHOD

| Method | Flops |
|--------|----------------------------|
| GCC | $(5rN/2) \log_2(rN)$ |
| FCC | $K(N + 2) + N + I(4K - 1)$ |

V. RESULTS

To evaluate the performance in realistic settings, the BIRD dataset [62], which provides numerous room impulse responses (RIRs) simulated using the image method, is used. In this dataset, simulations are performed in virtual rooms with width and length between 5 and 15 m, and height between 3 and 4 m. RIRs that correspond to an absorption coefficient of the surface between 0.2 and 0.8 are used, which leads to reverberation times RT60 between 0.10 and 1.00 sec that follow a gamma distribution [62]. The pair of microphones is positioned randomly in the virtual room, with a spacing between microphones that correspond to $d \pm 0.001$ m, where d lies in the range [0.01, 0.15] m. The sound source is positioned randomly, and kept at a distance between 1 and 5 m from the microphones. The speed of sound varies between 335 and 350 m/sec, to accomodate for different ambient temperatures. White noise is then convolved with the selected RIRs from BIRD to obtain the observed signals at both microphones. This simulation setup is similar to the one used for SVD-PHAT to measure accuracy [37].

The accuracy and computational load of FCC highly depends on the chosen low-rank decomposition order K . We set $\tau_{max} = 8$ to generate a set of bases \mathbf{P} which can accommodate for spacing up to $d = 0.15$ m between microphones at a

sample rate of $f_S = 16000$ samples/sec and a minimum speed of sound of $c = 335.0$ m/sec. The low-rank approximation is investigated for $K \in \{1, 2, \dots, 8\}$. GCC is also investigated to provide a baseline, with different time interpolation for $r \in \{1, 2, 4\}$. Quadratic interpolation is then performed to refine the TDoA estimation, and generate $\hat{\theta}_l$ as previously described in (5). The frame size $N = 512$ samples, with an overlap of 50% between frames and a smoothing factor of $\alpha = 0.1$. The mean absolute error (MAE) in degrees ($^\circ$) is then computed as follows:

$$\text{MAE} = \frac{1}{L} \sum_{l=1}^L |\theta_l - \hat{\theta}_l| \quad (23)$$

where L stands for the total number of TDoAs, and the angles θ_l and $\hat{\theta}_l$ correspond to:

$$\theta_l = \arccos\left(\frac{\tau_l c}{df_S}\right), \quad \hat{\theta}_l = \arccos\left(\frac{\hat{\tau}_l c}{df_S}\right). \quad (24)$$

Table II presents the mean absolute error (MAE) for GCC (with different values of r) and FCC (with different values of K), with RT60 values selected randomly at each simulation according to the distribution provided in the BIRD dataset [62]. The results demonstrate the need to increase the IFFT size (by doubling it, with $r = 2$) with GCC to obtain a good accuracy, due to the main lobe interpolation explained in Fig. 2. The accuracy difference between $r = 2$ and $r = 4$ is negligible, suggesting a larger r increases the computational load without improving the accuracy significantly. It is interesting to note that FCC with $K = 8$ can achieve a similar accuracy as GCC (with $r = 2$) for all configurations up to a distance of $d = 0.15$ m. Note that small values of K lead to large MAEs when distance between microphones increases. This error however reduces as the value of K increases.

The number of flops for each configuration can be calculated using the equations in Table I. For the same MAE, it shows that FCC (with $K = 8$) uses only 5647 flops instead of 25600 for GCC (with $r = 2$). This implies a theoretical reduction in computational load by a factor of 4.5. While the number of flops provides a rough estimation of the computational load, it ignores other factors such as the memory access time and the potential vector optimizations when the algorithm runs on a modern processor. To consider these factors, FCC is implemented in the C language¹ and runs on a Raspberry Pi Zero (ARM v7) [57], a Raspberry Pi 4 (Quad core Cortex-A72) [58] and a Nvidia Jetson TX2 (ARM Cortex-A57) [59] devices. Note that on the Nvidia Jetson TX2 the algorithm runs on the CPU and not the GPU. GCC runs on the same hardware, and uses the optimized FFTW library to compute the IFFT efficiently [60]. Both methods are compiled with the GNU Compiler Collection [63] and use vectorization. Table III shows that in practice with $M = 2$ microphones, FCC ($K = 8$) runs 8.2, 2.6 and 2.7 times faster than GCC ($r = 2$) for the Raspberry Pi Zero, Raspberry Pi 4 and Nvidia Jetson TX2, respectively. This confirms that FCC brings an important gain when deployed on low-cost hardware. The difference in these speed ratios and the ratio of the number of flops (4.5)

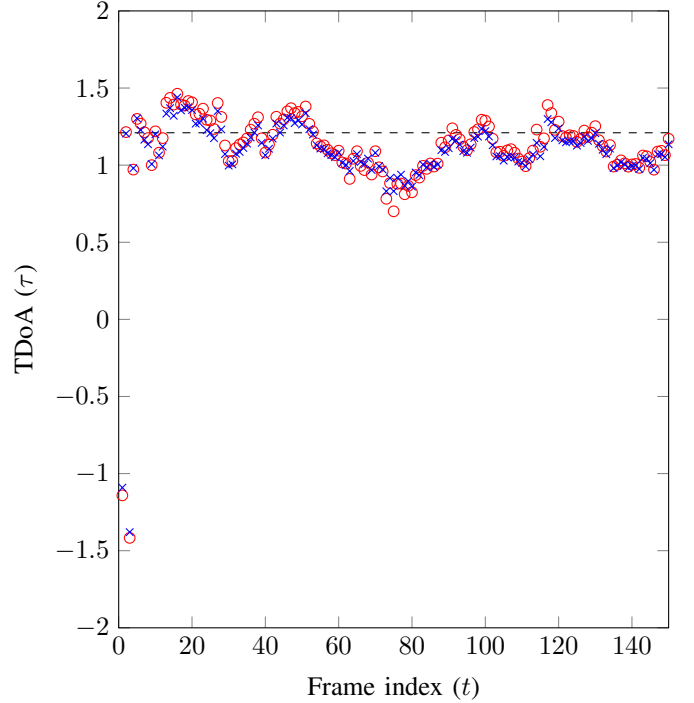


Fig. 5. Predicted TDoAs with GCC ($r = 2$) (○) and FCC ($K = 8$) (×), compared to the theoretical TDoA $\tau = 1.21$ (—).

in Table II comes from the fact that memory access also plays a role in execution time, and that FFTW is carefully optimized to run as fast as possible on various processors. Note that the most significant improvement is observed on the slowest hardware, the Raspberry Pi Zero, which suggests the proposed method is particularly effective for devices with little cache memory. Also note that the number of cross-correlation operations increases with a complexity $\mathcal{O}(M^2)$, where M stands for the number of microphones, as GCC or FCC is computed for each pair of microphones. As the number of microphones increases, the computational load associated to Step 2 (Cross Spectrum + PHAT) becomes significant. This suggests that further optimization of this specific step could reduce the overall amount of computations as future work.

Figure 5 compares the estimated TDoAs of GCC and FCC using their respective C implementation to estimate TDOAs for an example where the microphones are 5 cm apart, with the theoretical TDoA $\tau = 1.21$ and RT60 = 0.613 sec. Both plots show similar predicted TDoAs, which is a specific example that illustrates how both GCC and FCC perform with the same accuracy, while FCC requires less computations than GCC. The difference in the predictions between GCC and FCC comes mainly from the fact that the bases are limited to $K = 8$ for FCC.

VI. CONCLUSION

This paper introduces FCC, well-suited for microphone arrays with a small aperture (a few centimeters) by providing similar accuracy to GCC but outperforming it in terms of computational load. It demonstrates that the amount of flops between FCC and GCC is reduced by a factor of 4.5, and the

¹<https://github.com/francoisgrondin/fcc>

TABLE II
MEAN ABSOLUTE ERROR (MAE) IN DEGREES (°)

| Method | Parameter | Flops | Distance between microphones (d) (in m) | | | | | | | | | | | | | | |
|--------|-----------|-------|---------------------------------------------|-------------|-------------|------------|------------|------------|------------|------------|------------|------------|------------|------------|------------|------------|------------|
| | | | 0.01 | 0.02 | 0.03 | 0.04 | 0.05 | 0.06 | 0.07 | 0.08 | 0.09 | 0.10 | 0.11 | 0.12 | 0.13 | 0.14 | 0.15 |
| GCC | $r = 1$ | 11520 | 23.0 | 19.3 | 13.2 | 9.6 | 9.4 | 8.7 | 8.1 | 7.8 | 7.8 | 7.2 | 7.5 | 8.0 | 8.3 | 8.7 | 8.5 |
| | $r = 2$ | 25600 | 19.4 | 16.4 | 11.4 | 8.0 | 8.0 | 7.6 | 7.4 | 7.1 | 7.1 | 6.5 | 6.6 | 7.3 | 7.8 | 7.8 | 7.7 |
| | $r = 4$ | 56320 | 19.0 | 16.0 | 11.2 | 7.9 | 7.9 | 7.7 | 7.2 | 7.3 | 7.2 | 6.7 | 6.8 | 7.5 | 7.8 | 8.0 | 7.7 |
| FCC | $K = 1$ | 1125 | 21.4 | 20.3 | 17.1 | 14.4 | 20.3 | 26.5 | 28.6 | 29.4 | 29.7 | 29.2 | 28.1 | 27.5 | 26.9 | 29.5 | 29.4 |
| | $K = 2$ | 1771 | 19.7 | 17.8 | 13.3 | 9.5 | 10.1 | 10.4 | 11.9 | 15.6 | 17.9 | 18.7 | 19.7 | 20.5 | 20.8 | 23.1 | 24.2 |
| | $K = 3$ | 2417 | 20.8 | 19.0 | 14.4 | 9.6 | 8.6 | 8.8 | 9.4 | 10.0 | 10.9 | 12.5 | 14.2 | 14.7 | 15.9 | 18.0 | 19.6 |
| | $K = 4$ | 3063 | 19.4 | 17.0 | 12.4 | 8.9 | 9.2 | 8.7 | 7.9 | 8.3 | 8.9 | 8.9 | 9.7 | 10.7 | 12.8 | 14.7 | 16.7 |
| | $K = 5$ | 3709 | 20.3 | 17.9 | 12.8 | 8.4 | 8.2 | 8.1 | 8.0 | 7.7 | 7.2 | 7.1 | 8.0 | 8.7 | 9.4 | 10.7 | 12.6 |
| | $K = 6$ | 4355 | 19.2 | 16.4 | 11.7 | 8.5 | 8.4 | 7.8 | 7.4 | 7.5 | 7.6 | 6.9 | 7.1 | 7.6 | 8.4 | 8.9 | 9.0 |
| | $K = 7$ | 5001 | 19.9 | 17.1 | 11.9 | 8.1 | 8.0 | 8.0 | 7.6 | 7.1 | 7.0 | 6.6 | 6.9 | 7.5 | 7.7 | 8.1 | 7.9 |
| | $K = 8$ | 5647 | 19.2 | 16.3 | 11.4 | 8.1 | 7.9 | 7.6 | 7.3 | 7.3 | 7.2 | 6.5 | 6.7 | 7.4 | 7.9 | 7.8 | 7.4 |

TABLE III
EXECUTION TIME (μ SEC) PER FRAME WITH RESPECT TO HARDWARE AND NUMBER OF MICROPHONES (M)

| Step | Raspberry Pi Zero | | | Raspberry Pi 4 | | | Nvidia Jetson TX2 | | |
|----------------------------|-------------------|---------------|---------------|----------------|-------------|--------------|-------------------|-------------|--------------|
| | $M = 2$ | $M = 4$ | $M = 8$ | $M = 2$ | $M = 4$ | $M = 8$ | $M = 2$ | $M = 4$ | $M = 8$ |
| 1) STFT | 137.3 | 291.4 | 608.0 | 12.0 | 24.3 | 47.0 | 10.7 | 21.9 | 44.2 |
| 2) Cross Spectrum + PHAT | 35.6 | 239.8 | 1251.6 | 3.2 | 19.2 | 90.5 | 4.6 | 27.9 | 130.1 |
| 3) GCC ($r = 2$) | 206.0 | 1281.5 | 6246.1 | 9.8 | 57.6 | 268.5 | 8.4 | 53.4 | 236.1 |
| 4) FCC ($K = 8$) | 25.0 | 180.4 | 898.5 | 3.8 | 22.5 | 114.0 | 2.7 | 16.1 | 75.1 |
| 5) Quadratic Interpolation | 3.5 | 20.2 | 94.2 | 0.1 | 0.1 | 0.3 | 0.1 | 0.1 | 0.4 |
| Total with GCC (1+2+3+5) | 382.4 | 1832.9 | 8199.9 | 25.1 | 101.2 | 406.3 | 23.8 | 103.4 | 410.9 |
| Total with FCC (1+2+4+5) | 201.4 | 731.8 | 2852.3 | 19.1 | 66.1 | 251.8 | 18.1 | 66.0 | 250.3 |

execution time is reduced by a factor of 8.2, 2.6 and 2.7 on Raspberry Pi Zero, Raspberry Pi 4 and Nvidia Jetson TX2, respectively.

The next step consists in using FCC to estimate TDoAs for each pair of microphones in a microphone array, and to perform a search for the best DoA candidate. This functionality could be added to existing frameworks such as ODAS [27], and exploits optimization strategies introduced with SMP-PHAT for microphone arrays that show some symmetry [36]. We also plan to investigate multiple TDoAs estimation, using a similar approach to what is currently done with SVD-PHAT [64]. It would be also relevant to use time-frequency binary masks to improve TDoA estimation for a specific class of sound [65], [66], [67], [68]. We believe FCC can be a powerful building block for sound source localization with microphone arrays of arbitrary geometries.

REFERENCES

- J. Barker, R. Marxer, E. Vincent, and S. Watanabe, "The third CHiME speech separation and recognition challenge: Dataset, task and baselines," in *Proceedings of the IEEE Workshop on Automatic Speech Recognition and Understanding*, 2015, pp. 504–511.
- P. Pertilä, E. Cakir, A. Hakala, E. Fagerlund, T. Virtanen, A. Politis, and A. Eronen, "Mobile microphone array speech detection and localization in diverse everyday environments," in *Proceedings of the European Signal Processing Conference*, 2021, pp. 406–410.
- H. Tang, W.-N. Hsu, F. Grondin, and J. Glass, "A study of enhancement, augmentation, and autoencoder methods for domain adaptation in distant speech recognition," in *Proceedings of Interspeech*, 2018, p. 2928–2932.
- E. Tuncer and B. Friedlander, *Classical and modern direction-of-arrival estimation*. Academic Press, 2009.
- Z. Chen, G. Gokeda, and Y. Yu, *Introduction to Direction-of-arrival Estimation*. Artech House, 2010.
- A. S. Bregman, *Auditory scene analysis: The perceptual organization of sound*. MIT press, 1994.
- P. Pertilä, A. Brutti, P. Svaizer, and M. Omologo, "Multichannel source activity detection, localization, and tracking," *Audio source separation and speech enhancement*, pp. 47–64, 2018.
- E. A. P. Habets, J. Benesty, I. Cohen, S. Gannot, and J. Dmochowski, "New insights into the MVDR beamformer in room acoustics," *IEEE Transactions on Audio, Speech, and Language Processing*, vol. 18, no. 1, pp. 158–170, 2009.
- H. Erdogan, J. R. Hershey, S. Watanabe, M. I. Mandel, and J. Le Roux, "Improved MVDR beamforming using single-channel mask prediction networks," in *Proceedings of Interspeech*, 2016, pp. 1981–1985.
- F. Grondin, J.-S. Lauzon, J. Vincent, and F. Michaud, "GEV beamforming supported by DOA-based masks generated on pairs of microphones," in *Proceedings of Interspeech*, 2020, pp. 3341–3345.
- Z. Chen, X. Xiao, T. Yoshioka, H. Erdogan, J. Li, and Y. Gong, "Multi-channel overlapped speech recognition with location guided speech extraction network," in *Proceedings of the IEEE Spoken Language Technology Workshop*, 2018, pp. 558–565.
- R. Mazur and A. Mertins, "A sparsity based criterion for solving the permutation ambiguity in convolutive blind source separation," in *Proceedings of the IEEE International Conference on Acoustics, Speech and Signal Processing*, 2011, pp. 1996–1999.
- Z.-Q. Wang, J. Le Roux, and J. R. Hershey, "Multi-channel deep clustering: Discriminative spectral and spatial embeddings for speaker-

independent speech separation,” in *Proceedings of the IEEE International Conference on Acoustics, Speech and Signal Processing*, 2018, pp. 1–5.

[14] T. Higuchi, K. Kinoshita, M. Delcroix, K. Zmolíková, and T. Nakatani, “Deep clustering-based beamforming for separation with unknown number of sources,” in *Proceedings of Interspeech*, 2017, pp. 1183–1187.

[15] L. Drude and R. Haeb-Umbach, “Tight integration of spatial and spectral features for bss with deep clustering embeddings,” in *Proceedings of Interspeech*, 2017, pp. 2650–2654.

[16] P. Pertilä and J. Nikunen, “Distant speech separation using predicted time–frequency masks from spatial features,” *Speech communication*, vol. 68, pp. 97–106, 2015.

[17] S. U. Wood, J. Rouat, S. Dupont, and G. Pironkov, “Blind speech separation and enhancement with GCC-NMF,” *IEEE/ACM Transactions on Audio, Speech, and Language Processing*, vol. 25, no. 4, pp. 745–755, 2017.

[18] A. Maldonado, C. Rascon, and I. Velez, “Lightweight online separation of the sound source of interest through blstm-based binary masking,” *Computación y Sistemas*, vol. 24, no. 3, pp. 1257–1270, 2020.

[19] C. Rascon and I. Meza, “Localization of sound sources in robotics: A review,” *Robotics and Autonomous Systems*, vol. 96, pp. 184–210, 2017.

[20] S. Michaud, S. Faucher, F. Grondin, J.-S. Lauzon, M. Labbé, D. Létourneau, F. Ferland, and F. Michaud, “3D localization of a sound source using mobile microphone arrays referenced by SLAM,” in *Proceedings of the IEEE/RSJ International Conference on Intelligent Robots and Systems*, 2020, pp. 10402–10407.

[21] T. Yamada, K. Itoyama, K. Nishida, and K. Nakadai, “Sound source tracking by drones with microphone arrays,” in *Proceedings of the IEEE/SICE International Symposium on System Integration*, 2020, pp. 796–801.

[22] A. B. A. Qayyum, K. N. Hassan, A. Anika, M. F. Shadiq, M. M. Rahman, M. T. Islam, S. A. Imran, S. Hossain, and M. A. Haque, “DOANet: a deep dilated convolutional neural network approach for search and rescue with drone-embedded sound source localization,” *EURASIP Journal on Audio, Speech, and Music Processing*, vol. 2020, no. 1, pp. 1–18, 2020.

[23] J.-S. Lauzon, F. Grondin, D. Létourneau, A. L. Desbiens, and F. Michaud, “Localization of RW-UAVs using particle filtering over distributed microphone arrays,” in *Proceedings of the IEEE/RSJ International Conference on Intelligent Robots and Systems*, 2017, pp. 2479–2484.

[24] J. Kim, C. Park, J. Ahn, Y. Ko, J. Park, and J. C. Gallagher, “Real-time uav sound detection and analysis system,” in *Proceedings of the IEEE Sensors Applications Symposium*, 2017, pp. 1–5.

[25] I.-J. Jung and J.-G. Ih, “Acoustic localization and tracking of the multiple drones,” in *Proceedings of INTER-NOISE and NOISE-CON Congress and Conference*, vol. 259, no. 8, 2019, pp. 1373–1377.

[26] S. Michaud, B. Moffett, A. T. Rousiuk, V. Duda, and F. Grondin, “Smartbelt: A wearable microphone array for sound source localization with haptic feedback,” *arXiv preprint arXiv:2202.13974*, 2022.

[27] F. Grondin, D. Létourneau, C. Godin, J.-S. Lauzon, J. Vincent, S. Michaud, S. Faucher, and F. Michaud, “ODAS: Open embedded audition system,” *arXiv preprint arXiv:2103.03954*, 2021.

[28] K. Nakadai, H. G. Okuno, H. Nakajima, Y. Hasegawa, and H. Tsujino, “An open source software system for robot audition HARK and its evaluation,” in *Proceedings of the IEEE/RAS International Conference on Humanoid Robots*, 2008, pp. 561–566.

[29] H. Do, H. F. Silverman, and Y. Yu, “A real-time SRP-PHAT source location implementation using stochastic region contraction (SRC) on a large-aperture microphone array,” in *Proceedings of the IEEE International Conference on Acoustics, Speech and Signal Processing*, vol. 1, 2007, pp. 121–124.

[30] M. Cobos, A. Martí, and J. J. Lopez, “A modified SRP-PHAT functional for robust real-time sound source localization with scalable spatial sampling,” *IEEE Signal Processing Letters*, vol. 18, no. 1, pp. 71–74, 2010.

[31] C. Knapp and G. Carter, “The generalized correlation method for estimation of time delay,” *IEEE Transactions on Acoustics, Speech, and Signal Processing*, vol. 24, no. 4, pp. 320–327, 1976.

[32] J.-M. Valin, F. Michaud, and J. Rouat, “Robust localization and tracking of simultaneous moving sound sources using beamforming and particle filtering,” *Robotics and Autonomous Systems*, vol. 55, no. 3, pp. 216–228, 2007.

[33] J. H. DiBiase, H. F. Silverman, and M. S. Brandstein, “Robust localization in reverberant rooms,” in *Microphone arrays*. Springer, 2001, pp. 157–180.

[34] M. S. Brandstein and H. F. Silverman, “A robust method for speech signal time-delay estimation in reverberant rooms,” in *Proceedings of the IEEE International Conference on Acoustics, Speech, and Signal Processing*, vol. 1, 1997, pp. 375–378.

[35] F. Grondin and F. Michaud, “Lightweight and optimized sound source localization and tracking methods for open and closed microphone array configurations,” *Robotics and Autonomous Systems*, vol. 113, pp. 63–80, 2019.

[36] F. Grondin, M.-A. Maheux, J.-S. Lauzon, J. Vincent, and F. Michaud, “SMP-PHAT: Lightweight DoA estimation by mergin microphone pairs,” *arXiv preprint: arXiv:2203.14409*, 2022.

[37] F. Grondin and J. Glass, “SVD-PHAT: A fast sound source localization method,” in *Proceedings of the IEEE International Conference on Acoustics, Speech and Signal Processing*, 2019, pp. 4140–4144.

[38] ———, “Fast and robust 3-D sound source localization with DSVD-PHAT,” in *Proceedings of the IEEE/RSJ International Conference on Intelligent Robots and Systems*, 2019, pp. 5352–5357.

[39] R. Schmidt, “Multiple emitter location and signal parameter estimation,” *IEEE Transactions on Antennas and Propagation*, vol. 34, no. 3, pp. 276–280, 1986.

[40] F.-M. Han and X.-D. Zhang, “An ESPRIT-like algorithm for coherent doa estimation,” *IEEE Antennas and Wireless Propagation Letters*, vol. 4, pp. 443–446, 2005.

[41] C. T. Ishi, O. Chatot, H. Ishiguro, and N. Hagita, “Evaluation of a MUSIC-based real-time sound localization of multiple sound sources in real noisy environments,” in *Proceedings of the IEEE/RSJ International Conference on Intelligent Robots and Systems*, 2009, pp. 2027–2032.

[42] Y. Bando, Y. Masuyama, Y. Sasaki, and M. Onishi, “Robust auditory functions based on probabilistic integration of music and cgmm,” *IEEE Access*, vol. 9, pp. 38718–38730, 2021.

[43] K. Nakamura, K. Nakadai, F. Asano, Y. Hasegawa, and H. Tsujino, “Intelligent sound source localization for dynamic environments,” in *Proceedings of the IEEE/RSJ international conference on Intelligent Robots and Systems*, 2009, pp. 664–669.

[44] K. Nakamura, K. Nakadai, F. Asano, and G. Ince, “Intelligent sound source localization and its application to multimodal human tracking,” in *Proceedings of the IEEE/RSJ International Conference on Intelligent Robots and Systems*, 2011, pp. 143–148.

[45] K. Nakadai, G. Ince, K. Nakamura, and H. Nakajima, “Robot audition for dynamic environments,” in *Proceedings of the IEEE International Conference on Signal Processing, Communication and Computing*, 2012, pp. 125–130.

[46] K. Nakamura, K. Nakadai, and G. Ince, “Real-time super-resolution sound source localization for robots,” in *Proceedings of the IEEE/RSJ International Conference on Intelligent Robots and Systems*, 2012, pp. 694–699.

[47] S. Chakrabarty and E. A. Habets, “Broadband DOA estimation using convolutional neural networks trained with noise signals,” in *Proceedings of the IEEE Workshop on Applications of Signal Processing to Audio and Acoustics*, 2017, pp. 136–140.

[48] ———, “Multi-speaker DOA estimation using deep convolutional networks trained with noise signals,” *IEEE Journal of Selected Topics in Signal Processing*, vol. 13, no. 1, pp. 8–21, 2019.

[49] G. K. Papageorgiou, M. Sellathurai, and Y. C. Eldar, “Deep networks for direction-of-arrival estimation in low snr,” *IEEE Transactions on Signal Processing*, vol. 69, pp. 3714–3729, 2021.

[50] E. Ozanich, P. Gerstoft, and H. Niu, “A feedforward neural network for direction-of-arrival estimation,” *The journal of the acoustical society of America*, vol. 147, no. 3, pp. 2035–2048, 2020.

[51] Q. Li, X. Zhang, and H. Li, “Online direction of arrival estimation based on deep learning,” in *Proceedings of the IEEE International Conference on Acoustics, Speech and Signal Processing*, 2018, pp. 2616–2620.

[52] W. He, P. Motlicek, and J.-M. Odobez, “Neural network adaptation and data augmentation for multi-speaker direction-of-arrival estimation,” *IEEE/ACM Transactions on Audio, Speech, and Language Processing*, vol. 29, pp. 1303–1317, 2021.

[53] E. Çakir, G. Parascandolo, T. Heittola, H. Huttunen, and T. Virtanen, “Convolutional recurrent neural networks for polyphonic sound event detection,” *IEEE/ACM Transactions on Audio, Speech, and Language Processing*, vol. 25, no. 6, pp. 1291–1303, 2017.

[54] S. Adavanne, A. Politis, J. Nikunen, and T. Virtanen, “Sound event localization and detection of overlapping sources using convolutional recurrent neural networks,” *IEEE Journal of Selected Topics in Signal Processing*, vol. 13, no. 1, pp. 34–48, 2018.

[55] S. Adavanne, A. Politis, and T. Virtanen, “Direction of arrival estimation for multiple sound sources using convolutional recurrent neural net-

work," in *Proceedings of the European Signal Processing Conference*, 2018, pp. 1462–1466.

[56] F. Grondin, J. Glass, I. Sobieraj, and M. D. Plumley, "Sound event localization and detection using CRNN on pairs of microphones," *arXiv preprint arXiv:1910.10049*, 2019.

[57] R. Grimmett, *Getting Started with Raspberry Pi Zero*. Packt Publishing Ltd, 2016.

[58] S. McManus and M. Cook, *Raspberry Pi for dummies*. John Wiley & Sons, 2021.

[59] K. Rungsuptawekoon, V. Visoottiviseth, and R. Takano, "Evaluating the power efficiency of deep learning inference on embedded gpu systems," in *Proceedings of the International Conference on Information Technology*, 2017, pp. 1–5.

[60] S. G. Johnson and M. Frigo, "A modified split-radix FFT with fewer arithmetic operations," *IEEE Transactions on Signal Processing*, vol. 55, no. 1, pp. 111–119, 2006.

[61] M. Abe and J. O. Smith III, "Design criteria for simple sinusoidal parameter estimation based on quadratic interpolation of fft magnitude peaks," in *Proceedings of the Audio Engineering Society Convention*, 2004, pp. 1–13.

[62] F. Grondin, J.-S. Lauzon, S. Michaud, M. Ravanelli, and F. Michaud, "BIRD: Big Impulse Response Dataset," *arXiv preprint arXiv:2010.09930*, 2020.

[63] R. M. Stallman, *Using and porting the GNU compiler collection*. Free Software Foundation, 1999, vol. 86.

[64] F. Grondin and J. Glass, "Multiple sound source localization with svd-phat," in *Proceedings of Interspeech*, 2019, pp. 2698–2702.

[65] F. Grondin and F. Michaud, "Time difference of arrival estimation based on binary frequency mask for sound source localization on mobile robots," in *Proceedings of the IEEE/RSJ International Conference on Intelligent Robots and Systems*, 2015, pp. 6149–6154.

[66] ———, "Noise mask for TDOA sound source localization of speech on mobile robots in noisy environments," in *Proceedings of the IEEE International Conference on Robotics and Automation*, 2016, pp. 4530–4535.

[67] W. Mack, J. Wechsler, and E. A. Habets, "Signal-aware direction-of-arrival estimation using attention mechanisms," *arXiv preprint arXiv:2201.00503*, 2022.

[68] P. Pertilä and E. Cakir, "Robust direction estimation with convolutional neural networks based steered response power," in *Proceedings of the IEEE International Conference on Acoustics, Speech and Signal Processing*, 2017, pp. 6125–6129.



Marc-Antoine Maheux received his bachelor's degree ('19) in Computer Engineering from the Université de Sherbrooke (Québec, Canada). He is currently a Ph.D. student in Electrical Engineering at the Université de Sherbrooke (Québec, Canada). His research interests include social robotics, machine learning and intelligent systems. He is also closely involved in open source software design at IntRoLab (Intelligent / Interactive / Integrated / Interdisciplinary Robot Lab). He is a Candidate to the Engineering Profession (CEP) of OIQ (Ordre des ingénieurs du Québec).



Jean-Samuel Lauzon received his bachelor's degree ('16) and Master's degree ('19) in Electrical Engineering from the Université de Sherbrooke (Québec, Canada). He is currently a Ph.D. student in Electrical Engineering at the Université de Sherbrooke. His research interests include robot audition, signal processing and machine learning. He is a Candidate to the Engineering Profession (CEP) of OIQ (Ordre des ingénieurs du Québec).



Jonathan Vincent received his bachelor's degree ('16) and Master's degree ('20) in Electrical Engineering from the Université de Sherbrooke (Québec, Canada). He is currently a Ph.D. student in Electrical Engineering at the Université de Sherbrooke. His research interests include multimodal fusion, image recognition and machine learning. He is a Candidate to the Engineering Profession (CEP) of OIQ (Ordre des ingénieurs du Québec).



François Grondin received his bachelor's degree ('09) in Electrical Engineering from McGill University (Québec, Canada), and his Master's degree ('11) and Ph.D. degree ('17) in Electrical Engineering from the Université de Sherbrooke (Québec, Canada). After completing postdoctoral work ('19) in the Computer Science & Artificial Intelligence Laboratory (CSAIL) at Massachusetts Institute of Technology (Massachusetts, USA), he became a faculty member in the Department of Electrical Engineering and Computer Engineering of the Université de Sherbrooke. His research interests include robot audition, sound source localization, speech enhancement, sound classification and machine learning. He has published over 30 peer-reviewed papers in journals and international conferences. He is a member of IEEE and OIQ (Ordre des ingénieurs du Québec).

François Michaud received his bachelor's degree ('92), Master's degree ('93) and Ph.D. degree ('96) in Electrical Engineering from the Université de Sherbrooke (Québec, Canada). After completing postdoctoral work ('97) at Brandeis University (Massachusetts, USA), he became a faculty member in the Department of Electrical Engineering and Computer Engineering of the Université de Sherbrooke, and founded IntRoLab, a research laboratory working on designing intelligent autonomous systems that can assist humans in living environments. His expertise is in autonomous decision-making algorithms, human-robot interaction, user-interfaces, artificial vision and audition. He has extensive experience in initiating and conducting interdisciplinary research projects involving collaborators in physiotherapy, occupational therapy, child psychiatry, education, cognitive science, arts, automotive and manufacturing. He has published over 190 peer-reviewed papers in journals and international conferences, has been awarded 8 patents, and made significant open source (software and hardware) contributions used by the robotics community. Prof. Michaud held the Canada Research Chair (2001-11) in Mobile Robots and Autonomous Intelligent Systems, and is the founding Director of the Interdisciplinary Institute for Technological Innovation (3IT). He is also the founding director of the Quebec Strategic Cluster INTER (Interactive Technologies in Rehabilitation Engineering) and a graduate training program in Collaborative Robotics for the Manufacturing Sector. He is currently Director of the Bachelor of Robotics Engineering Program at the Université de Sherbrooke. He is a member of IEEE, AAAI and OIQ (Ordre des ingénieurs du Québec).